Inorg. Chem. **2008**, *47*, 5495−5502

Electrical Properties and Electronic States of Molecular Conductors Based on Unsymmetrical Organometallic-Dithiolene Gold(III) Complexes

Kazuya Kubo,*,† Akiko Nakao,‡ Yasuyuki Ishii,† Takashi Yamamoto,† Masafumi Tamura,† Reizo Kato,*,† Kyuya Yakushi,§ and Gen-etsu Matsubayashi|

RIKEN, JST-CREST, 2-1, Hirosawa, Wako-shi, Saitama 351-0198, Japan, KEK, 1-1 Oho, Tsukuba, Ibaraki 305-0801, Japan, Institute of Molecular Science, Myodaiji, Okazaki 444-8585, Japan, and Department of Molecular Chemistry Graduate School of Engineering, Osaka University, 2-1, Yamadaoka, Suita, Osaka 565-0871, Japan

Received January 29, 2008

The electronic properties of cation radical salts derived from organometallic mixed-ligand complexes [(ppy)Au(S−S)] (ppy^- = *C*-dehydro-2-phenylpyridine(−); $S-S^{2-}$ = dithiolene ligand) with Au(III)−C σ-bond were investigated. A 2:1 salt complex $[(ppy)Au(C_8H_4S_8)]_2[PF_6]$ ($C_8H_4S_8^{2-}$ = 2-{(4,5-ethylenedithio)-1,3-dithiole-2-ylidene}−1,3-dithiole-4,5-dithiolate(2−)) exhibited semiconductive behavior under ambient pressure (ρ_{rt} = 2.6 Ω cm, E_a = 0.03 eV). Magnetic measurements show that it is a Mott insulator close to the metal−insulator boundary. Raman and infrared spectra have revealed that the complex has a quasi-one-dimensional dimeric structure consisting of uniformly charged donor molecules. The complex exhibits metallic behavior at pressures above 0.8 GPa. In contrast, a similar compound $[(ppy)Au(C_8H_4S_6O_2)]_2[BF_4]$ ($C_8H_4S_6O_2^{2-}$ = 2-{(4,5-ethylenedioxy)-1,3-dithiole-2-ylidene}-1,3-dithiole-4,5-dithiolate(2−)) is a band insulator.

1. Introduction

Mixed-ligand−metal complexes possess various attractive features for application as efficient catalysts in organic synthesis, [1] building blocks of nanosize supramolecules,[2] and as switching and nonlinear optical devices.[3] However, only a few applications of mixed-ligand complexes[4] have been reported as conducting materials, although there are a large number of unsymmetrical organic donors.[5] In particular, a donor (HOMO)−metal−acceptor (LUMO) type molecule based on a mixed-ligand complex is capable of providing a new principle for the design of molecular conductors using the potential interplay of intra- and intermolecular charge transfers.

Matsubayashi et al. suggested that planar $[(N-N)M(S-S)]^{n+}$ ($M = Ni^{2+}$, Pd^{2+}, Pt^{2+}, Au^{3+}; N−N = diimine ligand; $S-S^{2-}$ = dithiolene ligand; n = 0 or 1) type unsymmetrical metal−dithiolene complexes would be good candidates for new components of molecular conductors.[6] The complexes, having HOMO on the dithiolene ligand and LUMO on the diimine ligand, are known to exhibit remarkable emission and luminescent spectra because of their unconventional electronic structures.[7] We have attempted to extend the field of conducting and magnetic materials by using of the unsymmetrical molecules. For this purpose, a series of diimine Pd^{2+}, Pt^{2+} complexes with $S-S^{2-}$ = $dmit^{2-}$

* To whom correspondence should be addressed. Fax: +81-48-462-4661. Phone: +81-48-467-9412. E-mail: kkubo@riken.jp (K.K.), reizo@riken.jp (R.K.).
† RIKEN, JST-CREST.
‡ KEK.
§ Institute of Molecular Science.
| Osaka University.

(1) (a) Labinger, J. A.; Bercaw, J. E. *Nature* **2002**, *417*, 507–514. (b) Miyaura, N.; Suzuki, A. *Chem. Rev.* **1995**, *95*, 2457–2483. (c) Noyori, R.; Ohkuma, T. *Angew. Chem., Int. Ed.* **2001**, *40*, 40–73.
(2) (a) Yamaguchi, T.; Tashiro, S.; Tominaga, M.; Kawano, M.; Ozeki, T.; Fujita, M. *J. Am. Chem. Soc.* **2004**, *126*, 10818–10819. (b) Takeda, N.; Umemoto, K.; Yamaguchi, K.; Fujita, M. *Nature* **1999**, *398*, 794–796. (c) Kumazawa, K.; Biradha, K.; Kusukawa, T.; Okano, T.; Fujita, M. *Angew. Chem., Int. Ed.* **2003**, *42*, 3909–3913.
(3) (a) Curreli, S.; Deplano, P.; Faulmann, C.; Ienco, A.; Mealli, C.; Mercuri, M. L.; Pilia, L.; Pintus, G.; Serpe, A.; Trogu, E. F. *Inorg. Chem.* **2004**, *43*, 5069–5079. (b) Albrecht, M.; van Koten, G. *Angew. Chem., Int. Ed.* **2001**, *40*, 3750–3781.
(4) Watanabe, E.; Fujiwara, M.; Yamaura, J.-I.; Kato, R. *J. Mater. Chem.* **2001**, *11*, 2131–2141.
(5) (a) Fable, J. M. *Chem. Rev.* **2004**, *104*, 5133–5150. (b) *TTF Chemistry-Fundamentals and Applications of Tetrathiafulvalene*; Yamada, J., Sugimoto, T., Ed.; Kodansha, Springer: Tokyo, 2004.
(6) (a) Matsubayashi, G.; Yamaguchi, Y.; Tanaka, T. *J. Chem. Soc., Dalton Trans.* **1988**, 2215–2219. (b) Matsubayashi, G.; Hirao, M.; Tanaka, T. *Inorg. Chim. Acta* **1988**, *144*, 217–221. (c) Nakahama, A.; Nakano, M.; Matsubayashi, G. *Inorg. Chim. Acta* **1999**, *284*, 55–60.

10.1021/ic800176q CCC: $40.75
Published on Web 05/13/2008

or $C_8H_4S_8^{2-}$ ($dmit^{2-}$ = 1,3-dithiole-2-thiol-4,5-dithiolate(2−), $C_8H_4S_8^{2-}$ = 2-{(4,5-ethylenedithio)-1,3-dithiole-2-ylidene}-1,3-dithiole-4,5-dithiolate(2−)) were prepared. For the Pd^{2+} and Pt^{2+} complexes, electrochemical or chemical oxidation yielded 1:1 radical cation salts such as $[(bpy)Pt(C_8H_4S_8)][BF_4]$ (bpy = 2,2′-bipyridine), which exhibited insulating behavior.[8] Au^{3+} complexes of this type were not obtained because of difficulties in the synthesis.[9]

To improve the conducting properties of the salts, the carbon−metal σ-bond was considered. Orthometalated chelating ligands, such as ppy^- (ppy^- = *C*-dehydro-2-phenylpyridine(−)), can modify the electronic structure of diimine complexes, because of its asymmetry and the strong σ-bonding of the phenyl carbon atom.[10] According to this strategy, new types of unsymmetrical organometallic donors $[(ppy)M(S-S)]^{n-}$ (M = Pt^{2+}, Au^{3+}; $S-S^{2-}$ = $C_8H_4S_8^{2-}$, $C_8H_4S_6O_2^{2-}$ = 2-{(4,5-ethylenedioxy)-1,3-dithiole-2-ylidene}-1,3-dithiole-4,5-dithiolate(2−); n = 0 or 1) were prepared.[11−13]

The distributions of the HOMO and LUMO in these orthometalated compounds are analogous to those of the diimine complexes.[14] However, the lowest charge transfer (CT) excited states of the square-planar d_8 complex $[(ppy)Au(C_8H_4S_8)]$ and $[(ppy)Pt(C_8H_4S_8)]^-$ are not similar to that of $[(bpy)Pt(C_8H_4S_8)]$ because of the orthometalation. In addition, the energies of the ground states for the orthometalated complexes are lower than those of the related diimine complexes.[11,13] Therefore, the σ-bond coordination markedly affects the HOMO and LUMO energy levels on the complexes.

This suggests that control of the intra- and intermolecular CT by the use of an organometallic compound containing a metal−carbon σ-bond may be a new way to construct conducting materials. The N−N-type complexes provided 1:1 salts that were insulators because of their high electron-donating abilities.[8] The carbon−metal σ-bond can be used to tune the electron-donating abilities of these types of unsymmetrical complexes, and control the band fillings of the salts.

Scheme 1. Unsymmetrical Organometallic Donors Containing a Metal−carbon Bond

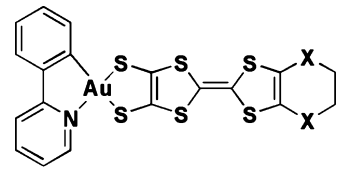

X = S: $[Au(ppy)(C_8H_4S_8)]$
X = O: $[Au(ppy)(C_8H_4S_6O_2)]$

Cation radical salts of the orthometalated complexes were successfully obtained by electrochemical or chemical oxidation. The salts of the orthometalated Pt complexes are insulators.[13] However, the salts of the Au(III) complexes with the σ-bond displayed peculiar conducting properties in comparison with the salts of other unsymmetrical complexes.

The unsymmetrical Au(III) complexes (Scheme 1) provided various 2:1 cation radical salts of the form $[(ppy)Au(S-S)]_2[Q][solvent]_n$ (Q = PF_6^-, BF_4^-, AsF_6^-, and TaF_6^-; solvent = PhCl and PhCN; n = 0−0.5) by electrochemical crystallization.[12,15,16] Among these, $[(ppy)Au(C_8H_4S_8)]_2[PF_6]$ (**1**) is a semiconductor under ambient pressure and shows metallic behavior under high pressure. To our knowledge, this is the first metallic molecular conductor based on unsymmetrical mixed-ligand organometallic complexes.

In this paper, we focus on the salts **1** and $[(ppy)Au(C_8H_4S_6O_2)]_2[BF_4]$ (**2**) and determine the correlation between their conducting properties and chemical structures. The crystals of these salts consist of similar 2-fold head-to-head stacking structures of cation radicals. However, they exhibit contrasting electrical properties. To elucidate the origin of this difference, the electronic states of these complexes are discussed on the basis of electrical conductivity, crystal structure, energy band calculations, Raman and infrared (IR) spectroscopy, and magnetic susceptibility. The optical and magnetic data show that **1** has a dimeric and quasi-one-dimensional structure, which is relevant to the electron correlation effect at ambient pressure. The band calculation suggests the possible origin of the pressure-induced metallic behavior of **1**.

2. Experimental Section

2.1. Preparation and Crystal Structure Determination of $[(ppy)Au(C_8H_4S_8)]_2[PF_6]$ (1) and $[(ppy)Au(C_8H_4S_6O_2)]_2[BF_4]$ (2). Single crystals of radical cation salts **1** and **2** and their precursor complexes were prepared by a previously reported method.[11,12,15,16] The chemical formula of the complex was determined by X-ray crystal structural analysis. Crystal structures were determined as described in the literature.[12,15]

2.2. Band Calculation. The intermolecular overlap integrals (S) between the frontier orbitals were calculated on the basis of the

(7) (a) Miller, T. R.; Dance, I. G. *J. Am. Chem. Soc.* **1973**, *95*, 6970–6979. (b) Vogler, A.; Kunkely, H.; Hlavatsch, J.; Merz, A. *Inorg. Chem.* **1984**, *23*, 506–509. (c) Zuleta, J. A.; Bevilacqua, J. M.; Proseripio, D. M.; Harvey, P. D.; Eisenberg, R. *Inorg. Chem.* **1992**, *31*, 2396–2404. (d) Paw, W.; Cummings, S. D.; Mansour, M. A.; Connick, W. B.; Geiger, D. K.; Eisenberg, R. *Coord. Chem. Rev.* **1998**, *171*, 125–150. (e) Cocker, T. M.; Bachman, R. E. *Inorg. Chem.* **2001**, *40*, 1550–1556. (f) Makedonas, C.; Mitsopoulou, C. A.; Lahoz, F. J.; Balana, A. I. *Inorg. Chem.* **2003**, *42*, 8853–8865. (g) Chen, C.-T.; Liao, S.-Y.; Lin, K.-J.; Chen, C.-H.; Lin, T.-Y. J. *Inorg. Chem.* **1999**, *38*, 2734–2741.
(8) (a) Kubo, K.; Nakano, M.; Tamura, H.; Matsubayashi, G. *Inorg. Chim. Acta* **2000**, *311*, 6–14. (b) Kubo, K.; Nakano, M.; Tamura, H.; Matsubayashi, G. *Inorg. Chim. Acta* **2002**, *336*, 120–124.
(9) Kubo, K. Unpublished work.
(10) (a) Mdleleni, M. M.; Bridgewater, J. S.; Watts, R. J.; Ford, P. C. *Inorg. Chem.* **1995**, *34*, 2334–2342. (b) Schmid, B.; Garces, F. O.; Watts, R. J. *Inorg. Chem.* **1994**, *33*, 9–14. (c) Craig, C. A.; Watts, R. J. *Inorg. Chem.* **1989**, *28*, 309–313. (d) Ichimura, K.; Kobayashi, T.; King, K. A.; Watts, R. J. *J. Phys. Chem.* **1987**, *91*, 6104–6106. (e) Ohsawa, Y.; Sprouse, S.; King, K. A.; DeArmond, M. K.; Hanck, K. W.; Watts, R. J. *J. Phys. Chem.* **1987**, *91*, 1047–1054. (f) Sprouse, S.; King, K. A.; Spellane, P. J.; Watts, R. J. *J. Am. Chem. Soc.* **1984**, *106*, 6647–6653. (g) Meyers, G. F.; Hall, M. B.; Chinn, J. W.; Lagow, R. J. *J. Am. Chem. Soc.* **1985**, *107*, 1431–1432.
(11) Kubo, K.; Nakano, M.; Tamura, H.; Matsubayashi, G.; Nakamoto, M. *J. Organomet. Chem.* **2003**, *669*, 141–148.
(12) Kubo, K.; Nakao, A.; Ishii, Y.; Kato, R.; Matsubayashi, G. *Synth. Met.* **2005**, *153*, 425–428.
(13) Suga, Y.; Nakano, M.; Tamura, H.; Matsubayashi, G. *Bull. Chem. Soc. Jpn.* **2004**, *77*, 1877–1883.
(14) Mansour, M. A.; Lachicotte, R. J.; Gysling, H. J.; Eisenberg, R. *Inorg. Chem.* **1998**, *37*, 4625–4632.
(15) Kubo, K.; Nakano, M.; Tamura, H.; Matsubayashi, G. *Eur. J. Inorg. Chem.* **2003**, *409*, 3–4098.
(16) Kubo, K.; Nakao, A.; Ishii, Y.; Tamura, M.; Kato, R.; Matsubayashi, G. *J. Low Temp. Phys.* **2006**, *142*, 413–416.

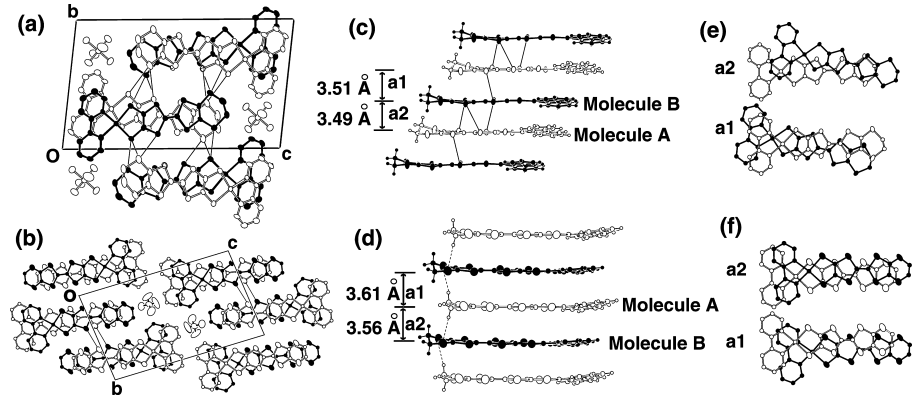

Figure 1. Crystal structures depicted on the basis of the results described in refs 12 and 15. Packing diagrams of (a) **1** and (b) **2** viewed along the *a* axis. Side-views of the columns in the crystals of (c) **1** and (d) **2** (see also Table 1). Molecular arrangements between molecules A and B in the column of the crystals for (e) **1** and (f) **2**. Fine lines indicate S···S contacts shorter than 3.7 Å. Dashed lines indicate O···H contacts within the range of 2.62−2.70 Å.

extended Hückel molecular orbital (MO) method. The semiempirical parameters for the Slater-type atomic orbitals were taken from the literature.[17]

2.3. Electrical Resistivity. The temperature dependence of the electrical resistivity was measured by the standard four-probe method at ambient pressure for **1** and **2**. Gold wires (10 μm diameter) were attached to the crystal with carbon paste. High-pressure resistivity measurements of **1** were also performed in the range from 0.2 to 1.6 GPa using a clamp-type piston-cylinder high-pressure cell.[18] The actual pressures at low temperature were determined by measurement of the shift of the superconducting transition temperature of Sn set in the pressure cell together with the sample.

2.4. Raman and IR Reflectance Spectra. Polarized reflectance spectra were obtained using a Nicolet Magna 760 FT-IR spectrometer combined with a Spectratech IR-Plan microscope. The spectral resolution was 4 cm^{-1}. The light polarization was set parallel ($\parallel a$) and perpendicular ($\perp b^*$) to the stacking directions in the two-dimensional (2-D) sheets or almost parallel to the *c* axis, which is almost along the long axis of the [(ppy)Au($C_8H_4S_8$)] molecule. Conductivity spectra were obtained by application of the Kramers−Kronig transformation to the reflectance spectra. Raman spectra were measured using a Renishaw Raman microscope system in the backward-scattering configuration, with irradiation by a 780 nm laser. No spectral changes were observed when a 633 nm laser was used. The intensity of the excitation light was reduced below 0.1 mW to avoid radiation damage. The incident light was polarized, but no polarizer was applied to the scattered light. The spectral resolution was 2 cm^{-1}.

2.5. Magnetic Susceptibility. Magnetic susceptibility of **1** (6.72 mg) was measured under a magnetic field of 5 T using a superconducting quantum interference device (SQUID) magnetometer (Quantum Design, MPMS-XL7) in the temperature range of 1.7−300 K. Magnetic anisotropy was also measured for a mosaic of 30 single crystals of **1** (1.8 mg) aligned in the same direction and attached using Apiezon N grease under the same magnetic field and temperature range.

3. Results and Discussion

3.1. Structural Features of 1 and 2. In our previous reports, details of the crystal structures of **1** and **2** were already discussed.[12,15] The following are the crystallographic data for **1**: chemical formula, $C_{38}H_{24}Au_2F_6N_2PS_{16}$; crystal system, triclinic; space group, $P\bar{1}$; a = 8.2731(2) Å; b = 12.8828(5) Å; c = 21.6185(7) Å; α = 83.375(1)°; β = 87.937(1)°; γ = 85.809(2)°; Z = 2. That for **2** follows: chemical formula, $C_{38}H_{24}Au_2BF_4N_2O_4S_{12}$; crystal system, triclinic; space group, $P\bar{1}$; a = 7.316(2) Å; b = 13.250(4) Å; c = 22.868(7) Å; α = 82.509(8)°; β = 80.75(1)°; γ = 83.71(1)°; Z = 2.[12,15] In this report, the experimental results are discussed on the basis of these crystal structures. For both crystals, the asymmetric unit contains two cations and one anion. Two crystallographically independent molecules, A and B, are indicated by the white and black bond drawings in Figure 1. Columnar structures are formed by 2-fold head-to-head stacking of the cation radicals in the manner ···ABAB··· (Figure 1a) and b). Figure 1c and d shows side-views of the columns. Significant differences were found in the distances between the molecular planes. This difference corresponds to the different overlapping modes in **1** and **2**, as shown in Figure 1e and f. The intermolecular interactions between oxygen and hydrogen atoms in $C_8H_4S_6O_2$ are observed along the stacking direction in **2** (Figure 1d).[19] For **1**, many intermolecular S···S contacts (3.339−3.616 Å) shorter than the van der Waals distance (<3.7 Å) are found along the column, as well as between the columns (Figure 1a). However, only the intercolumn S···S contacts are observed in **2** (3.686 Å, Figure 1b).

3.2. Electrical Resistivity. Figure 2 shows the temperature dependence of the resistivity of **1** under various pressures. Salt **1** exhibits semiconductive behavior with a small activation energy (ρ_{rt} = 2.6 Ω cm; E_a = 0.03 eV) at ambient pressure. Metallic behavior appears above 0.8 GPa. At 1.6 GPa, **1** is metallic down to a temperature of 20 K. On the other hand, salt **2** is highly insulating ($\rho_{rt} > 1 \times 10^5$ Ω cm) at ambient pressure and room temperature. To our knowledge, salt **1** is the first example of an organometallic

(17) (a) Summerville, R. H.; Hoffmann, R. *J. Am. Chem. Soc.* **1976**, *98*, 7240–7254. (b) Hoffman, D. M.; Hoffmann, R.; Fisel, C. R. *J. Am. Chem. Soc.* **1982**, *104*, 3858–3875. (c) Hoffmann, R.; Howell, J. M.; Rossi, A. R. *J. Am. Chem. Soc.* **1976**, *98*, 2484–2492. (d) Chen, M. M. L.; Hoffmann, R. *J. Am. Chem. Soc.* **1976**, *98*, 1647–1653.

(18) (a) Walker, I. R. *Rev. Sci. Instrum.* **1999**, *70*, 3402–3412. (b) Ishii, Y.; Tamura, M.; Kato, R.; Hedo, M.; Uwatoko, Y.; Môri, N. *Synth. Met.* **2005**, *152*, 389–392.

(19) Horiuchi, S.; Yamochi, H.; Saito, G.; Sakaguchi, K.-I.; Kusunoki, M. *J. Am. Chem. Soc.* **1996**, *118*, 8604–8622.

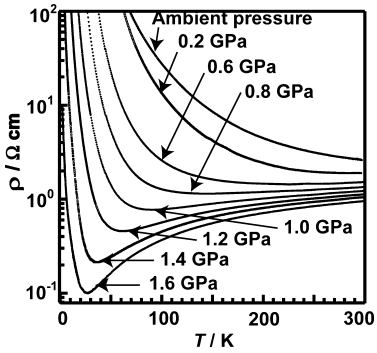

Figure 2. Temperature dependence of the resistivity of **1** at various pressures, from ambient pressure to 1.6 GPa.

compound (a system containing a metal−carbon bond) that exhibits metallic conduction behavior, even though pressure is required to achieve this state.

The application of pressure controls the electronic structure by changing the intermolecular interactions, as observed for other molecular conductors.[20–22] However, a detailed mechanism for this behavior depends on the origin of the insulating state at ambient pressure. For example, the change in dimensionality is significant for a density-wave insulator, whereas the role of bandwidth is dominant for a simple Mott insulator because of the electron correlation effect. In view of the pressure experiments, **1** is in the vicinity of the metal−insulator boundary. A question now arises; how can **1** become metallic by increased pressure, while **2** is a typical insulator? To answer this, the electronic band structures of these salts are examined in the next section. It is shown that the insulating state of **1** is not very stable against the change in intermolecular interactions; not only the bandwidth, but also other band features are suggested as being responsible for the pressure-induced metallic state. The character of the insulating state of **1** is further discussed on the basis of spectroscopic and magnetic studies.

3.3. Energy Band Calculations. The energy band structures of **1** and **2** were calculated using the tight-binding method with extended Hückel MO on the basis of the structural data. The energy band calculation for **1** was previously reported.[15] However, the result provided was irrelevant because wrong parametrization was used in the calculation and because of an incorrect determination of the symmetry points. Therefore, the revised results are reported here.

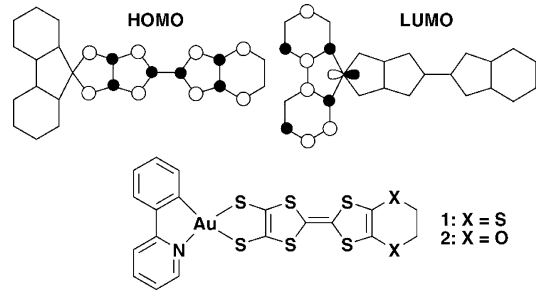

Figure 3. Calculated HOMO and LUMO for the cation moieties of **1** and **2**.

Figure 3 shows the HOMO and LUMO for the cation moieties of **1** and **2**. The HOMO is on the dithiolene ligand and the LUMO is on the ppy ligand. The results are consistent with the electronic absorption spectra of the precursor compound of **1**.[11] As with the π-donor molecules, BEDT-TTF and BO (BEDT-TTF = bis(ethylenedithio)tetrathiafulvalene; BO = bis(ethylenedioxio)tetrathiafulvalene), the HOMOs of **1** and **2** are characterized by the same signs on all the sulfur atoms.[19,23] This feature is advantageous for a donor molecule for the formation of a wide and less one-dimensional conduction band.

The calculated overlap integrals (S) between the HOMOs are listed in Table 1. Figure 4 shows the calculated energy bands formed from the HOMOs. The band calculation for **2** (Figure 4b) is consistent with the highly insulating behavior of **2**. Strong dimerization is evident in **2**; one of the face-to-face interactions (a2) is much stronger than the other (a1). The oxygen−hydrogen interactions in **2** are responsible for the strong dimerization in the stack. The dimerization causes a wide gap between the upper two (iii and iv in Figure 4b) and the lower two (i and ii) sub-bands, which correspond to the antibonding and bonding states of the dimer, respectively. The strong dimerization results in a considerable reduction

Table 1. Calculated overlap integrals (S) between HOMOs for the cation radical salts **1** and **2**

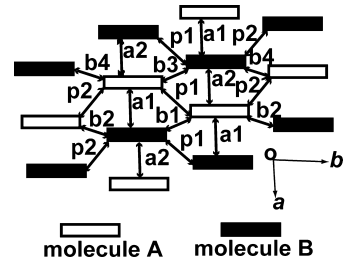

S ($\times 10^{-3}$)	1	2
a1	−8.3	−0.8
a2	−9.0	−4.6
b1	1.3	−0.2
b2	−1.9	−0.4
b3	1.1	−1.5
b4	−1.2	−0.2
p1	−1.2	−0.7
p2	−0.9	−0.2

(20) (a) Jérome, D.; Mazaud, A.; Ribault, M.; Bechgaard, K. *J. Phys., Lett.* **1980**, *41*, L95–L98. (b) Creuzet, F.; Jérome, D.; Moradpour, A. *Mol. Cryst. Liq. Cryst.* **1985**, *119*, 297–302. (c) Jérome, D. *Science* **1991**, *252*, 1509–1514.

(21) (a) Taniguchi, H.; Miyashita, M.; Uchiyama, K.; Satoh, K.; Môri, N.; Okamoto, H.; Miyagawa, K.; Kanoda, K.; Hedo, M.; Uwatoko, Y. *J. Phys. Soc. Jpn.* **2003**, *72*, 468–471. (b) Kini, A. M.; Geiser, U.; Wang, H. H.; Carlson, K. D.; Williams, J. M.; Kwok, W. K.; Vandervoort, K. G.; Thompson, J. E.; Stupka, D. L.; Jung, D.; Whangbo, M.-H. *Inorg. Chem.* **1990**, *29*, 2555–2557. (c) Williams, J. M.; Kini, A. M.; Wang, H. H.; Carlson, K. D.; Geiser, U.; Montgomery, L. K.; Pyrka, G. J.; Watkins, D. M.; Kommers, J. M.; Boryschuk, S. J.; Crouch, A. V. S.; Kwok, W. K.; Schirber, J. E.; Overmyer, D. L.; Jung, D.; Whangbo, M.-H. *Inorg. Chem.* **1990**, *29*, 3272–3274.

(22) (a) Brossard, L.; Ribault, M.; Valade, L.; Cassoux, P. *Phys. B+C* **1986**, *143*, 378–380. (b) Bousseau, M.; Valade, L.; Legros, J.-P.; Cassoux, P.; Carbauskas, M.; Interrante, L. V. *J. Am. Chem. Soc.* **1986**, *108*, 1908–1916. (c) Kato, R. *Chem. Rev.* **2004**, *104*, 5319–5346.

(23) (a) Mori, T.; Kobayashi, A.; Sasaki, Y.; Kobayashi, H.; Saito, G.; Inokuchi, H. *Bull. Chem. Soc. Jpn.* **1984**, *57*, 627–633. (b) Kobayashi, H.; Kato, R.; Mori, T.; Kobayashi, A.; Sasaki, Y.; Saito, G.; Inokuchi, H. *Mol. Cryst. Liq. Cryst.* **1985**, *125*, 125–134. (c) Shibaeva, R. P.; Yagubskii, E. B. *Chem. Rev.* **2004**, *104*, 5347–5378.

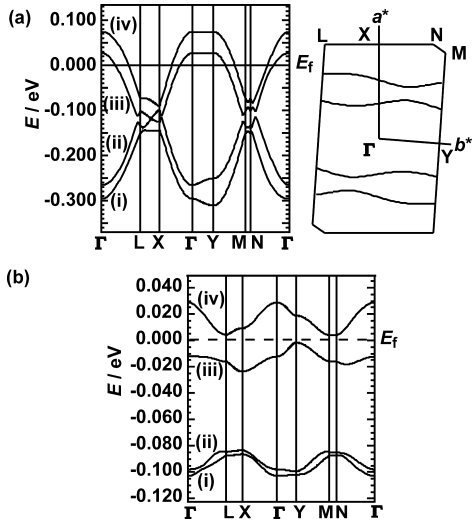

Figure 4. Calculated band structures and Fermi surface for (a) **1** and (b) **2**. Γ−X and Γ−Y lines denote the a^* and b^* axes, respectively, and L, M, N are the corners on the boundary of the first Brillouin zone.

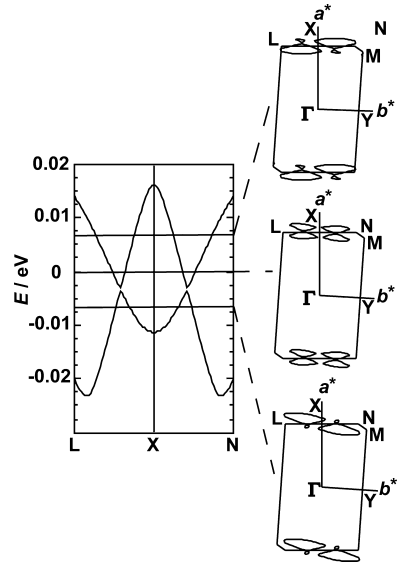

Figure 5. Close-up of the band structure of **1** around the band contact and an equi-energy contour map of the band structure viewed along the c^* axis at various energy levels.

of the widths of these sub-bands. The upper sub-bands (iii and iv) are further separated from each other, because one of the intercolumn interactions (b3) is dominant. Consequently, **2** is expected to be a band insulator. In real space, the dominant intercolumn interaction (b3) corresponding to the short S···S contacts (Figure 1b), links two dimers to compose a closed-shell tetramer, in which two holes are localized. In **2**, the intracolumn CH···O contacts (a2) and the intercolumn S···S contacts (b3) cooperate to form localized intermolecular bonds rather than conduction pathways, unlike the CH···O interactions in the BO salt that assist the formation of a two-dimensional conduction network.[19]

Crystal **1** also has a quasi-one-dimensional character (Figure 4a); the face-to-face interactions (a1 and a2) are larger than the side-by-side interactions (b1−b4, p1−p2). Although dimerization is found along the stacking in **1**, it is not as strong as that in **2**. As a result, **1** retains wider bands. The alternation of the intercolumn interactions along the *b* axis affords the separation between the sub-bands iii and iv (Figure 4a). In contrast to **2**, the sub-bands of **1** are much wider than this separation, so that both of the two upper sub-bands cross the Fermi level. Therefore, **1** is expected to be metallic in the framework of this band calculation; however, **1** is a semiconductor at ambient pressure. Experimental results described in the following sections rule out the possibility of a charge-density-wave insulating state because of the quasi-one-dimensional character or a charge ordered insulating state because of intersite Coulombic interactions. On the other hand, the band calculation for **1** suggests that the two upper sub-bands (iii and iv) are in a state close to effectively half-filled as a total, which plays a significant role associated with the effective on-site Coulombic interactions on the dimer unit. When sufficiently strong on-site Coulombic interactions operate in the half-filled system, the system is in a Mott insulating state.

The above band-structure calculation suggests that an increase in interdimer interactions can easily change **1** into a nonhalf-filled metallic state by either of two possible mechanisms; the overlap of sub-bands ii and iii or the separation of sub-bands iii and iv. In fact, metallic conduction is observed under pressure, as described in section 3.1.

If the second and third sub-bands (ii and iii) hybridize well with each other around the X point at the zone boundary, the effectively half-filled state changes to 3/4-filled. Therefore, this closing of the dimerization gap would provide a significant effect on the physical properties of **1**. The gap closing means that the dimerization is as weak as the intercolumn interactions. For isolated stacks with weak dimerization, a narrow gap opens at $k_a^* = \pi$ (XL line), where there is in-phase coupling of the antibonding levels of the dimers (sub-band iii) and that is situated slightly higher than the antiphase coupling of the bonding levels (sub-band ii). The intercolumn interactions decrease or raise these energies depending on k_b^*, so that the two sub-bands cross around the X point (Figure 5). This band crossing is not caused by the crystal symmetry. As shown in section 3.4, Raman and IR spectra indicate dimerization. Therefore, it appears that the band crossing is an artifact of the calculation and **1** has a gap between the sub-bands ii and iii, which means that the intracolumn dimerization is stronger than that expected from the calculation. However, on the basis of the result of the calculation, we consider that the gap is not so wide.

The separation between the two upper sub-bands (iii and iv) can also modify the filling condition. If the separation is sufficiently large, the two sub-bands can deviate from the half-filling to stabilize a semimetallic state. As determined from the experimental results in the following sections, the intercolumn interactions in **1** are not so large, which leads to the effectively half-filled condition and the Mott insulating state at ambient pressure.

It is difficult to conclude only from the present experiments whether the pressure-induced metallic state is accompanied by deviation from the half-filled state or not. For further study of this point, the radical cation salt of an unsymmetrical

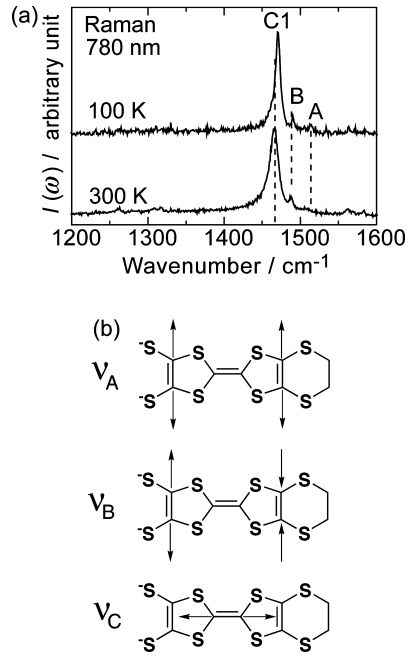

Figure 6. (a) Raman spectra of **1** at 300 and 100 K. (b) Schematic views of the three fundamental C═C stretching modes of the dithiolene moiety of the donor molecule in **1**. The stretching modes are labeled as ν_B and ν_C according to assignments of oxidized BEDT-TTF by Kozlov et al. in ref 24.

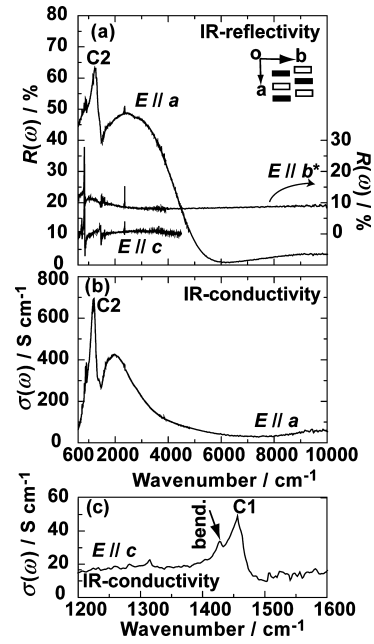

Figure 7. (a) Polarized IR reflectance spectra of **1** at 300 K. (b) Conductivity spectrum along the *a* axis ($E \parallel a$) at 300 K. (c) Close-up of the $E \parallel c$ conductivity spectrum at 300 K. The peak indicated by "bend." is due to the bending mode of the terminal ethylene group.

complex donor [(bpy)Pt($C_8H_4S_8$)] would be interesting because it takes the formal charge of +1 in the salt and crystallizes in a structure similar to **1**.[8]

3.4. Raman and IR Spectra. Figure 6a shows the Raman spectra of **1** measured at 300 and 100 K. Three peaks, A (ν_A = 1520 cm^{-1}), B (ν_B = 1490 cm^{-1}), and C1 (ν_{C1} = 1460 cm^{-1}), are commonly found in the spectra and are assigned to C═C stretching modes of the dithiolene unit, except that peak A is broadened at 300 K. These peaks do not shift by variation in temperature, indicating that the molecular charges do not change from 300 to 100 K. In addition, no change in the spectrum at 10 K was found when a 633 nm laser was used (data not shown). The dithiolene ligand of the donor molecule has a common moiety with the BEDT-TTF molecule. According to the assignment of the vibrational modes of neutral and oxidized BEDT-TTF by Kozlov et al.,[24] the peaks A, B, and C1 in Figure 6b can be simply ascribed to the three fundamental C═C stretching modes, ν_2, ν_{27}, and ν_3, of the BEDT-TTF moiety, respectively. Therefore, the peaks A and B are sensitive to the molecular charge, whereas peak C1 is not. Since no further splitting was observed in the spectra, all the donor molecules in **1** are uniformly charged with +0.5. If this is the case, the difference $\nu_A - \nu_2$ should be identical to $\nu_B - \nu_{27}$. This condition is in fact satisfied, that is, $\nu_{diff} = \nu_A - \nu_2 \approx \nu_B - \nu_{27} \approx +20$ cm^{-1}, where ν_2 and ν_{27} for BEDT-TTF$^{+0.5}$ are adopted. At least for these modes, the vibrational character of the donor molecule is in accord with that of BEDT-TTF. The linear relation between the frequencies of ν_2 and ν_{27} and the molecular charge has been established for BEDT-TTF, which results in the shift of ν_2 and ν_{27} by the molecular charge as ~ -120 cm^{-1}/hole and ~ -140 cm^{-1}/hole.[25] The donor charge of +0.5 in **1** is inferred from this, when a ν_{diff} value of +20 cm^{-1} is taken into account. A uniform donor charge of +0.5 is concluded from the Raman spectra and corresponds to the Mott insulating character of **1** based on the +1 charge of the dimers.

Figure 7a shows the IR reflectance spectra of **1** along three polarizations. In the $E \parallel c$ spectra, only sharp vibrational peaks are distinct, and the electronic contribution is negligible. The electronic contribution of the *b**-polarized spectra is finite but very small below 2000 cm^{-1}. On the other hand, the reflectance $R(\omega)$ spectrum for $E \parallel a$ exhibits a broad maximum around 2500 cm^{-1}. The quasi-one-dimensional electronic structure of **1** is evident. From the in-plane anisotropy, $E \parallel a$ versus $E \parallel b^*$, the ratio of the intercolumn to intracolumn interactions, t_{inter}/t_{intra}, is at most 1/10, or less, in **1**, where t_{inter} represents the average of the absolute transfer integrals labeled by b1−b4, p1, and p2 in Table 1, and t_{intra} is the absolute average of those labeled a1 and a2 in Table 1. Note that the *c* axis is not completely perpendicular to the stacking direction, *a*, which is responsible for the weak dispersion found in the $E \parallel c$ spectra.

The reflectance $R(\omega)$ spectrum for $E \parallel a$ exhibits three distinct features: a broad maximum around 2500 cm^{-1} accompanied by an edge structure below 6000 cm^{-1}, a marked peak structure at 1100 cm^{-1} (C2 in Figure 7a), and a low-wavenumber portion below 800 cm^{-1}, showing a monotonic decrease in $R(\omega)$ with the decrease in ω. These features indicate that **1** is a quasi-one-dimensional semicon-

(24) (a) Kozlov, M. E.; Pokhodnia, K. I.; Yurchenko, A. A. *Spectrochim. Acta* **1987**, *43A*, 323–329. (b) Kozlov, M. E.; Pokhodnia, K. I.; Yurchenko, A. A. *Spectrochim. Acta* **1989**, *45A*, 437–444.

(25) Yamamoto, T.; Uruichi, M.; Yamamoto, K.; Yakushi, K.; Kawamoto, A.; Taniguchi, H. *J. Phys. Chem. B* **2005**, *109*, 15226–15235.

ductor with an evidently dimeric structure. The broad maximum of $R(\omega)$ provides a broad peak at 2000 cm^{-1} in the conductivity spectrum $\sigma(\omega)$ for $E \parallel a$ obtained by Kramers−Kronig analysis of the $R(\omega)$ data, as shown in Figure 7b. This mid-IR peak of σ mainly contains the intradimer CT transition, that is, bonding−antibonding excitations from the two lower bands to the two upper bands, as typically observed in the dimerized BEDT-TTF salts such as β-(BEDT-TTF)$_2$X.[26] The appearance of the broad vibronic peak, C2, is also consistently explained by the CT transitions occurring in a dimeric structure. The C2 peak is attributed to the electron−molecular vibration (e−mv) coupling mode. The IR intensity of this mode is induced by the intradimer CT coupled to the out-of-phase vibration of the two molecules in the dimer. The feature appears for the polarization along the dimerization direction ($E \parallel a$), which is also analogous to the dimeric BEDT-TTF salt.[26] On the other hand, the C1 peak appearing in the $E \parallel c$ spectrum is associated with the in-phase vibration of the central C═C stretching mode in the dimer. The frequency of the C1 peak should be almost equal to that at a molecular charge of +0.5 because of the negligible contribution of interdimer CT in this polarization. For a symmetric molecule such as BEDT-TTF, the ν_3 mode without the e−mv coupling is IR inactive. In contrast, for the present case, a less perturbed peak is observed in the $E \parallel c$ spectrum (Figure 7c) at the same wavenumber, C1, as that in the Raman spectra (Figure 6a). The less perturbed C1 peak in the IR spectrum is ascribed to the unsymmetrical donor molecule. The C1 peak is negligible in the $E \parallel a$ spectrum, whereas the C2 peak has strong intensity (Figure 7a). This polarization dependence indicates that a pseudoinversion center exists on the dimer. The shift of the C2 peak from the C1 peak is −360 cm^{-1}. The shift is in quantitative agreement with the model calculations,[25] which provides the largest shift for a uniformly charged dimer. The large shift of C2 from C1 because of the e−mv coupling, is a manifestation of the uniform charges of the donor molecules.

The low-ω portion of the $\sigma(\omega)$ spectrum contains the interdimer CT contributions. The monotonic decrease of $R(\omega)$ below 800 cm^{-1} results in a rapidly descending $\sigma(\omega)$ with decreasing ω (Figure 7b), which indicates the charge gap opening at the Fermi level. This is consistent with the Mott insulating behavior of **1**.

From the present spectroscopic measurements, it was concluded that **1** at ambient pressure is a Mott insulator on the basis of the dimers of the donor molecules with a charge of +0.5, as shown in Figure 8. This is consistent with the symmetry observed in the X-ray diffraction measurement and the absence of satellite diffraction associated with the charge-density-wave formation.[27]

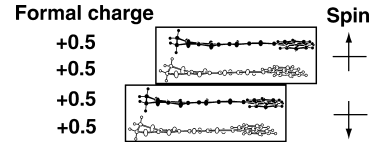

Figure 8. Schematic display of the electronic structure of **1** at ambient pressure.

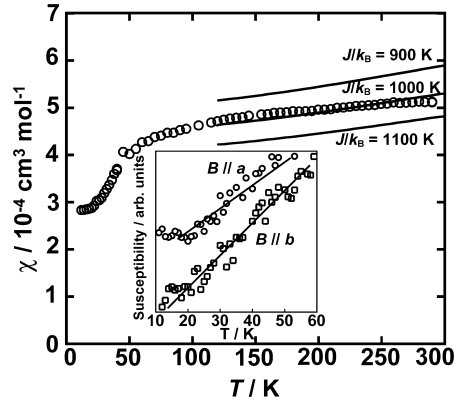

Figure 9. Temperature dependence of the paramagnetic susceptibility of **1**. Solid lines are those calculated for the antiferromagnetic one-dimensional Heisenberg model with J/k_B = 900, 1000, and 1100 K. The anisotropic susceptibility of the salt for a mosaic of oriented crystals is shown in the inset. The solid lines in the inset are given to indicate the line trends.

3.5. Magnetic Susceptibility. Magnetic measurements also provided evidence for the Mott insulating character of **1**. The temperature dependence of the paramagnetic susceptibility (χ) of **1** is shown in Figure 9. The χ value of **1** is 5.1 × 10^{-4} cm^3 mol^{-1} at room temperature, and gradually decreases to 4.0 × 10^{-4} cm^3 mol^{-1} on cooling to 50 K, where a change in the slope of $\chi(T)$ is observed. This behavior suggests that **1** is a low-dimensional paramagnetic insulator with large antiferromagnetic coupling, J, above 50 K, rather than a nonmagnetic band insulator. The magnetic susceptibility, as well as the vibrational spectra, indicates that **1** is an effectively half-filled system with $S = 1/2$ spin localized on each dimer $[(ppy)Au(C_8H_4S_8)]_2$ at ambient pressure (see Figure 8). The nonzero χ value extrapolated to $T = 0$ is consistent with the uniform arrangement of the dimers along the chain.

Below 50 K, χ decreases more rapidly to 2.8 × 10^{-4} cm^3 mol^{-1} at 12 K. This suggests a magnetic phase transition around 50 K. In fact, χ measured for the aligned crystals indicates anisotropy (Figure 9 inset); χ for the field along the b axis exhibits a steeper decrease than those for the other field directions. This indicates that the antiferromagnetic transition occurs at around 50 K, with an easy axis near the b direction. This supports the correlation effect in **1** which affords a paramagnetic Mott insulating state with significant antiferromagnetic coupling.

To estimate J, the susceptibility was analyzed above 50 K, assuming a one-dimensional antiferromagnetic Heisenberg model, $H = J\Sigma_j S_j S_{j+1}$, where the summation runs along the

(26) (a) Tajima, H.; Yakushi, K.; Kuroda, H.; Saito, G. *Solid State Commun.* **1985**, *56*, 159–163. (b) Jacobsen, C. S.; Tanner, D. B.; Williams, J. M.; Geiser, U.; Wang, H. H. *Phys. Rev. B* **1987**, *35*, 9605–9613.

(27) Conditions for the X-ray crystallographic analysis of **1** are described in ref 15.

(28) (a) Bonner, J. C.; Fisher, M. E. *Phys. Rev.* **1964**, *135*, A640–A658. (b) Eggert, S.; Affleck, I.; Takahashi, M. *Phys. Rev. Lett.* **1994**, *73*, 332–335. (c) Shiroishi, M.; Takahashi, M. *Phys. Rev. Lett.* **2002**, *89*, 117201/1–117201/4.

one-dimensional chain.[28] The susceptibilities calculated for this model with $J/k_B = 900$, 1000, and 1100 K were plotted and compared to the experimental results (solid lines in Figure 9). The overall behavior is approximately explained by $J/k_B \approx 10^3$ K, as estimated from this analysis, although the agreement was not very good. Even if the interchain couplings are also taken into consideration for improvement of the analysis, the value would be of the same order.

The value of J attests that the system is in the vicinity of the metal−insulator boundary as follows: the exchange coupling J is related to U_{dimer} and t as $J \approx t^2/U_{dimer}$ and to the insulating limit, $U_{dimer} \gg t$, where U_{dimer} denotes the effective on-site Coulombic repulsion within the dimer, and t represents the interdimer transfers. The overlap calculations for **1** indicate that the transfer integrals along the chain are of the order $t/k_B \approx 10^3$ K. If this is the case, $U_{dimer} \approx t^2/J$ is of the same order of magnitude $U_{dimer}/k_B \approx 10^3$ K. This estimation contradicts the condition, $U_{dimer} \gg t$; therefore, the system should be in the vicinity of the metal−insulator boundary, that is, $U_{dimer} \approx t$. This result agrees with the electrical resistivity measurements, which show that **1** easily becomes metallic under pressure (Figure 2).

Conclusions

The physical properties of molecular conductors based on unsymmetrical mixed-ligand organometallic−dithiolene gold(III) complexes with a carbon−metal σ-bond were investigated. It was demonstrated that an organometallic compound can have metallic conduction, which is an extension of π-electron-based conducting material design. Salt **1** behaves as a semiconductor under ambient pressure and as a metal under high pressure. To our knowledge, this is the first molecular conductor based on organometallic complexes (with a carbon−metal bonding) that exhibits metallic conduction. The role of the dithiolene ligands was analyzed in reference to the crystal structures and the band calculations. It was found the CH···O and the S···S contacts coexisting in the crystal are significant, both in creating conduction pathways and in localization. From the spectroscopic studies, no charge ordering was found, and the electronic state of **1** was determined as quasi-one-dimensional Mott insulator on the basis of dimers of uniformly charged donor molecules with a site-charge of +0.5. The magnetic study indicated that the ground-state of **1** is an antiferromagnetic Mott insulating state in the vicinity of the metal−insulator boundary. The band calculations suggest that the pressure-induced metallic state in salt **1** could be associated with the deviation from the half-filled state, as well as with the enhancement of the bandwidth.

Acknowledgment. We thank Dr. T. Miyazaki (National Institute for Materials Science in Japan) for the first principle calculation. This work was partially supported by a Grant-in-Aid for Scientific Research (No. 16GS0219) from the Ministry of Education, Culture, Sports, Science and Technology of Japan.

IC800176Q